molecular pharmaceutics

Article

Cite This: Mol. Pharmaceutics 2018, 15, 3236−3251

Phase Behavior of Drug-Hydroxypropyl Methylcellulose Amorphous Solid Dispersions Produced from Various Solvent Systems: Mechanistic Understanding of the Role of Polymer using Experimental and Theoretical Methods

Naila A. Mugheirbi,[†] Laura I. Mosquera-Giraldo,[†] Carlos H. Borca,[‡,§] Lyudmila V. Slipchenko,[‡] and Lynne S. Taylor*[,†]

[†]Department of Industrial and Physical Pharmacy, College of Pharmacy, Purdue University, 575 Stadium Mall Drive, West Lafayette, Indiana 47907, United States

[‡]Department of Chemistry, College of Science, Purdue University, 560 Oval Drive, West Lafayette, Indiana 47907, United States

Supporting Information

ABSTRACT: The vast majority of studies evaluating amorphous solid dispersions (ASDs) utilize solvent evaporation techniques as the preparation method. However, the impact of the solvent/cosolvent system properties on the polymer conformation and the phase behavior of the resultant drug/polymer blends is poorly understood. Herein, we investigate the influence of solvent properties on the phase behavior of ASDs containing itraconazole (ITZ) and hydroxypropylmethyl cellulose (HPMC) prepared using spin coating from binary/ternary cosolvent systems containing alkyl alcohols, dichloromethane (DCM), and water. The compatibility of the polymer with the cosolvent system was probed using high-resolution imaging techniques supported by molecular dynamics simulations. Solvent evaporation and evaporation rate profiles were tracked gravimetrically to understand the impact of the solvent composition on the evaporation process. Short-chain alcohols, including methanol (MeOH) and ethanol (EtOH), were found to induce drug-polymer demixing in the presence of water, with EtOH being less sensitive to moisture than MeOH owing to its ability to form an azeotrope with water. In contrast, water-induced mixing was observed when higher alcohols, including *n*-propanol (PrOH) and *n*-butanol (BuOH), were used as a cosolvent, due to the improved solubility of HPMC in the higher alcohols in the presence of water. Isopropanol (IPA) produced phase separated ASDs under wet and dry conditions with an increase in miscibility with faster evaporation rates in the presence of water. This solvent-triggered phase behavior highlights the importance of conducting a thorough screening of various solvents prior to the preparation of ASDs via solvent evaporation approaches such as spray drying.

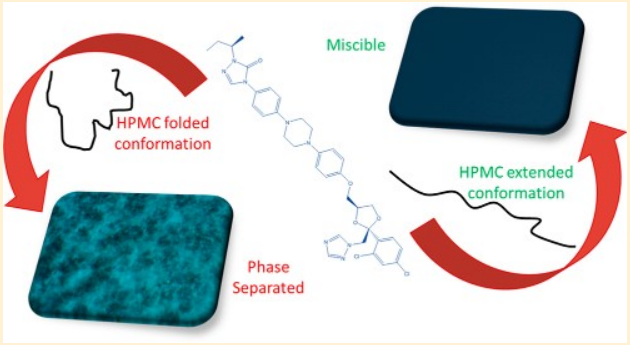

KEYWORDS: *itraconazole, alkyl alcohols, evaporation rate, amorphous solid dispersion, spin coating*

Downloaded via GEORGIA INST OF TECHNOLOGY on September 6, 2018 at 18:41:30 (UTC).
See https://pubs.acs.org/sharingguidelines for options on how to legitimately share published articles.

1. INTRODUCTION

Formulations containing active pharmaceutical ingredients (APIs) in amorphous form provide great potential to overcome bioavailability issues associated with poorly soluble APIs. The solubility advantage of the amorphous form of an API is attributed to their higher free energy and subsequently improved dissolution relative to crystalline forms, which can result in the formation of a supersaturated solution.[1] However, amorphous drugs tend to convert to the thermodynamically stable crystalline state with time.[2] To inhibit crystallization from the solid and solution states, amorphous drugs are usually blended with a suitable polymer, producing what is termed an amorphous solid dispersion (ASD).[3]

The physical stability of a given amorphous solid dispersion is highly dependent on the solubility of the crystalline form and/or the miscibility of the amorphous phase of the drug in the polymeric matrix. That is to say, if the drug loading is lower than the crystalline solubility, the system is thermodynamically stable, and therefore, no crystallization will take place. However, such low drug loadings are typically impractical.[4,5] On the other hand, if the drug loading exceeds the amorphous miscibility limit, amorphous−amorphous phase separation (AAPS) is thermodynamically favored, leading to the formation of a drug-rich phase and a polymer-rich phase. As a result, crystallization can take place in the drug-rich domains,

Received: March 26, 2018
Revised: June 4, 2018
Accepted: June 6, 2018
Published: June 6, 2018

 © 2018 American Chemical Society

DOI: 10.1021/acs.molpharmaceut.8b00324
Mol. Pharmaceutics 2018, 15, 3236−3251

which will ultimately compromise any solubility and dissolution rate enhancements of the formulation.[6]

Understanding the phase behavior of polymer/polymer and drug/polymer blends has attracted a great deal of interest over the past decade. Most studies conducted to understand phase behavior of blends have employed solvent evaporation techniques for fabrication. However, only a limited number of these studies has focused on the impact of the compatibility of the solvent system with the polymer on the phase behavior of the resultant blend; the majority of work in this area has focused on polymer mixtures.[7−9] The substantial difference in physicochemical properties between drug and polymer and the subsequent solubility gap between the two components in a given solvent system is expected to induce solvent-triggered variations in phase behavior.[10] Such solvent-induced phase variation is more complicated for ASDs prepared from multicomponent solvent systems as compared to those prepared from a single-solvent system.[11] However, the use of more than one solvent is common during pharmaceutical processing. In this respect, understanding the correlation between solvent composition, polymer conformation, and blend miscibility is of utmost importance for drug/polymer systems. While some studies have evaluated the influence of solvent composition on drug/polymer miscibility using techniques such as differential scanning calorimetry (DSC) and polarized light microscopy (PLOM),[8] these are low-resolution techniques which may lead to overestimation of drug/polymer miscibility.[12]

The itraconazole (ITZ)/hydroxypropyl methyl cellulose (HPMC) system has been reported to be phase separated when produced via solvent evaporation from DCM/MeOH under uncontrolled humidity conditions.[12] Recently, we have correlated the origin of the reported phase separation to the presence of water during the ASD production step.[13] The objective of this study was to carry out a thorough investigation of the impact of initial solvent composition on the polymer conformation and, as a result, the phase behavior of ITZ/HPMC ASDs produced using spin coating. To this end, five alkyl alcohols, methanol (MeOH), ethanol (EtOH), isopropanol (IPA), *n*-propanol (PrOH), and *n*-butanol (BuOH), were used as cosolvents with DCM. High-resolution characterization techniques were employed to investigate the phase behavior of the resultant amorphous films and to understand the underlying phenomena controlling the behavior of each solvent system.[13−15]

2. MATERIALS AND EXPERIMENTAL SECTION

2.1. Materials. Itraconazole (ITZ) was purchased from Attix Pharmaceuticals (Ontario, Canada); methanol, ethanol, isopropanol, *n*-propanol, *n*-butanol, and dichloromethane were purchased from Fischer Chemicals (NJ, U.S.A.). METHOCEL E3 grade was a gift from Dow Chemical Co. (Midland, MI).

2.2. Preparation of Drug/Polymer Stock Solutions. A set of stock solutions containing ITZ/HPMC in different solvents was prepared by dissolving a 30:70 w/w ITZ/HPMC blend in a 50:50 v/v mixture of each alkyl alcohol [MeOH, EtOH, IPA, *n*-PrOH, and *n*-BuOH] and DCM to have 10 mg/mL of total solid content in solution.

2.3. Preparation of Spin-Coated Films. A 100 μL aliquot of solution was spin coated on various substrates via dynamic dispensing using a two-step procedure (500 rpm for 3 s and 2000 rpm for 30 s as reported previously[13]) at 21, 30, 35, 40, and 50 °C using a heat assisted spin coating setup. A heat lamp, serving as a heat source, was placed above the sample zone of a KW-4A spin coater (Chemat Technology Inc., CA, U.S.A.), and the temperature was monitored using an infrared thermometer gun (VWR, Randor, PA) with environmental relative humidity (RH) maintained at 50 ± 5% RH.

A two-step, slower spinning speed was also assessed (500 rpm for 15 s and 500 rpm for 15 s) at various temperatures: 21, 30, 35, 40, and 50 °C. Following spin coating, all samples were stored under vacuum for at least 24 h to ensure complete removal of the solvent.

To investigate the texture of HPMC films produced under dry and wet conditions, a 7 mg/mL solution of HPMC E3 solution in a 1:1 mixture of DCM/alkyl alcohol was prepared and filtered using a 0.22 PTFE filter. The solution was then divided into two samples, where an aliquot (100 μL) of one sample was spin coated under a nitrogen purge (dry evaporation), and an aliquot of the second sample was spin coated at 50% RH (wet evaporation). Spin-coated HPMC films were then left to dry overnight, and the texture of these films was investigated using AFM.

2.4. Film Characterization. *2.4.1. Fluorescence Microscopy (FLOM).* Spin-coated films on a quartz substrate were imaged using an Olympus BX-51 fluorescence microscope (NY, U.S.A.) equipped with an excitation filter to provide an excitation wavelength of 330−380 nm and an emission filter to permit emitted wavelengths from 420 nm onward to be detected. The exposure time was set to 0.2 s and a 100× objective lens was used for all samples.

2.4.2. Transmission Electron (TE) Microscopy. TE micrographs were acquired using a FEI Tecnai G 20 electron microscope equipped with an LaB6 source and operated at 200 keV (Hillsboro, OR, U.S.A.). Samples were prepared by spin coating onto 300 mesh carbon-coated copper TEM grids with a standard thickness (5−6 nm) (SPI supplies, West Chester, PA), followed by incubation under vacuum overnight to remove residual solvents.

2.4.3. Topographical Imaging. A NanoIR2 AFM-IR instrument (Anasys Instruments, Inc., Santa Barbara, CA) was used to assess the topography of the spin-coated films. Contact mode NIR2 probes (model: PR-EX-NIR2, Anasys Instruments, Inc., Santa Barbara, CA) were used to collect AFM topographical images. A scan rate of 0.4 Hz was used for contact mode with an *x*- and *y*-resolution of 256 points. Topographical images were collected using the Analysis Studio software (version 3.10.5539). Lorentz contact resonance (LCR) spectroscopy and imaging was performed to evaluate the distribution of drug and polymer within the film based on the variation in the contact stiffness between the probe and the sample as described before.[13] A Thermalever probe (Model: EXP-AN2−300, Anasys Instruments Inc., Santa Barbara, CA) was used together with a small LCR drive magnet to conduct LCR sweeps and collect height and LCR images. LCR sweeps were then conducted to collect nanomechanical spectra of the area of interest. The spectra were collected between 1 and 200 kHz at a 100 kHz/s scan rate. A drive strength of 20% was used for LCR sweeps. In addition to nanomechanical spectra collection, LCR images were obtained by driving the AFM cantilever at the contact resonance mode of one of the components. The LCR drive strength was set to 50% to collect LCR images. The *x*- and *y*-resolution values were set at 256 and 256 pt, and the scan rate was 0.3 Hz. Localized nanothermal (nanoTA) measurements were also carried out. Temperature calibration was performed using three crystalline

DOI: 10.1021/acs.molpharmaceut.8b00324
Mol. Pharmaceutics 2018, 15, 3236−3251

polymers with melting points covering the entire temperature range of interest. The polymers used were polycaprolactone ($T_{melting}$ = 55 °C), polyethylene ($T_{melting}$ = 116 °C), and polyethylene terephthalate ($T_{melting}$ = 235 °C). A ThermaLever probe (model EXP-AN2−200, Anasys Instruments Inc., Santa Barbara, CA) was used in the contact mode. The probe was placed on the area of interest, and the AFM tip was heated linearly with time, and the bending of the probe was recorded. The temperature at which a thermal event, defined as penetration of the probe into the surface of the sample due to sample softening, occurs is taken as an indication of the glass transition for disordered substances.[16]

2.4.4. Determination of Temperature Dependent Solubility of Itraconazole. The solubility of ITZ in the investigated alcohols as a function of temperature was determined using heat/cool cycles with temperature control achieved using a Crystal 16 Parallel Crystallizer (Avantium, Amsterdam, Netherlands). Slurries of different ITZ concentrations (1−5.5 mg/mL) in various alcohols were prepared in 1 dram clear glass vials. The vials were then placed in the Crystal 16, heated to a given temperature (5 degrees below the alcohol boiling point) at 0.5 °C/min with continuous stirring at 300 rpm, and the clear point was recorded. The temperature was then reduced to 10 °C at 0.5 °C/min with the stirring maintained for the entire duration of the experiment, and the cloud point was recorded. Once the cloud point was reached, the suspension was filtered using a Whatman 2.5 μm filter (Vernon Hills, IL, U.S.A.). and the collected material was analyzed using DSC and PXRD.

2.4.5. Modulated Differential Scanning Calorimetry (MDSC). Approximately 3−5 mg of a powdered sample was analyzed using a DSC Q2000 differential scanning calorimeter (TA Instruments, Wood Dale, IL, U.S.A.) in a Tzero aluminum pan with a crimped lid. Samples were heated from 25 to 200 °C using a 5 °C/min heating rate, ± 0.796 modulation amplitude, and a 60 s modulation period. The data were analyzed using Universal Analysis (version 4.7A) software.

2.4.6. Thermal Gravimetric Analysis. The evaporation profile of the corresponding pure solvent mixtures were measured using a TGA Q50 thermogravimetric analyzer (TA Instruments, Wood Dale, IL, U.S.A.). Approximately 50 μL of each solution was placed into a tared platinum pan immediately prior to placement inside a temperature-controlled furnace (24 ± 0.5 °C) constantly purged with nitrogen at a 60 mL/min flow rate. The weight loss was recorded every minute until complete evaporation of the solvent occurred, which was confirmed by the absence of additional weight loss for at least 10 min. The derivative of percentage weight loss as a function of time is presented as the evaporation rate of the system.

2.5. Dynamic Light Scattering. The hydrodynamic diameter of HPMC in the solvent mixture before and after evaporation under dry conditions and at 50% RH was analyzed using a Nano-Zetasizer (Nano-ZS) from Malvern Instruments (Westborough, MA) equipped with dispersion technology software as described before.[8] A backscatter detector was used, and the scattered light was detected at an angle of 173°. A 7 mg/mL solution of HPMC E3 solution in a 1:1 mixture of DCM/alkyl alcohol was filtered using a 0.22 PTFE filter prior to DLS analysis. The solution was then divided into two samples, where one sample was left to evaporate under a nitrogen purge (dry evaporation), while the second sample was left to evaporate at 50% RH (wet evaporation). Both solutions, wet and dry evaporation, were left to evaporate until approximately 50% of the original volume had been evaporated. An aliquot (700 μL) of the solution was placed in a glass cuvette, and the size of polymer molecules/aggregates was measured. The reported values are the average of at least four measurements. Peaks with intensities below 5% were excluded from the plot.

2.6. Powder X-ray Diffraction. Powder X-ray diffraction (PXRD) of the filtrate collected immediately following the observation of the cloud point in the Crystal 16 experiments was carried out using a Rigaku SmartlabTM diffractometer (Rigaku Americas, The Woodlands, TX) with a Cu Kα radiation source (λ = 1.542 Å) and a D/teX Ultra detector. Glass sample holders were used, and diffraction patterns were obtained from 5−40° 2θ at a scan speed of 10°/min and a step size of 0.02°. The voltage and current used were 40 kV and 44 mA, respectively.

3. THEORETICAL CONSIDERATIONS

3.1. Hansen Solubility Parameters. The key consideration for selecting the proper solvent/solvent mixture for a polymer/polymer mixture is solubility. The internal energy of each component, i.e., that of the solvent and the polymer, is one of the factors impacting the solubility of the polymer in that solvent. Theoretically, polymer solubility can be predicted using the three-dimensional Hansen solubility parameters (HSP). The total solubility parameter, δ, of a polymer, as proposed by Hansen, can be calculated as the sum of squares of the partial solubility parameters, as shown in eq 1[17]

$$\delta = (\delta_{di}^2 + \delta_{pi}^2 + \delta_{hi}^2)^{1/2} \quad (1)$$

where the partial solubility parameters consist of δ_{di} accounting for dispersion or nonpolar effects, δ_{pi} accounting for polar effects, and δ_{hi} accounting for the hydrogen bonding nature of the species. The total solubility parameter of a polymer is a point located in three-dimensional space. This point is the center of a sphere called Hansen solubility sphere with radius R_0 referred to as the interaction radius of that polymer (Figure 1).

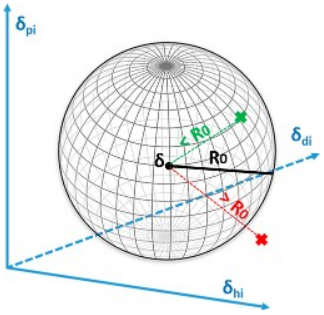

Figure 1. Schematic illustration of the Hansen's solubility sphere theory.

Eq 1 is used to calculate solubility parameters of solvents. For solvent mixtures, solubility parameters can be calculated using the following equation

$$\delta_{mixture} = \Phi_1\delta_1 + \Phi_2\delta_2 + \ldots \quad (2)$$

where Φ is the volume fraction of a mixture component.

DOI: 10.1021/acs.molpharmaceut.8b00324
Mol. Pharmaceutics 2018, 15, 3236−3251

Table 1. Structural Information for the Polymer Chain Resembling the Composition of HPMC E3 LV[a]

	monomer																			
position	1	2	3	4	5	6	7	8	9	10	11	12	13	14	15	16	17	18	19	20
C2	H	H	M	M	H	H	H	M	H	M	H	P	H	M	H	H	H	H	M	H
C3	H	M	H	H	M	P	H	H	H	M	M	H	H	H	P	M	H	M	H	H
C6	H	M	P	H	H	H	M	H	P	H	H	H	M	H	M	H	M	P	M	H

[a]The substituents are denoted as methoxyl (M), hydroxypropoxyl (P), and hydroxyl (H). There are three sites that can be substituted in each of the 20 monomers. Sites are denoted as C2, C3, and C6, according to the position in the HPMC monomer.

The distance between the total solubility parameter of the solvent and the total solubility parameter of the polymer (R_{ps}) can be calculated using the following equation[17]

$$R_{ps} = [4(\delta_p - \delta_s)^2_{di} + (\delta_p - \delta_s)^2_{pi} + (\delta_p - \delta_s)^2_{hi}]^{1/2} \quad (3)$$

where the "p" terms correspond to the parameters of the polymer, and the "s" terms to the parameters of the solvent. If the R_{ps} value is less than the radius of interaction (R_0) for the polymer, the solvent or solvent blend is expected to dissolve the polymer (green point in Figure 1) and vice versa (red point in Figure 1).[18]

In many cases, improved solvent quality can be achieved by choosing a solvent closer to the center of the volume of the solubility sphere for a given polymer resulting in improved solubility.[17,19] This can be achieved by adding a sufficient amount of an additional solvent, which is located in the direction one wants to move the total solubility parameter of the solvent mixture toward. That is, to move it toward the center of the polymer's solubility sphere. This concept was proposed by Hansen (1967) and is based on the assumption that no specific interactions take place between the components and that the solvent displacement is through additive solubility parameters based on their volume fraction.[17]

Although solubility parameters cannot be used to quantitatively predict the solubility of the polymer in each solvent, they were used herein to assess the potential miscibility of the polymer with each alcohol. The interaction radius and the HSP distance between the polymer and various alcohols were calculated using the values provided on the Hansen's solubility parameters web site.[20] The HSP distance upon mixing various alcohols with various fractions of water was also calculated based on volume fractions as described in eq 2 using the three-dimensional solubility parameters reported before.[21]

3.2. Molecular Dynamics Simulations. To gather information regarding the dynamics of an HPMC polymer chain in different solvent compositions, atomistic molecular dynamics (MD) simulations were performed in the molecular modeling package GROMACS 5.0, using the CHARMM classical force field.[22−24]

(1) A protein data bank (PDB) file containing structural information for the ethanol molecule was obtained from Networks/Pajek. The PDB file for *n*-propanol was retrieved from virtualchemistry.org.[25] The PDB files of IPA and DCM were extracted from the NIST Chemistry Webbook.

(2) The structures of ethanol, propanol, IPA, and DCM were submitted to the online topology building tool SwissParam to obtain their corresponding topology files in GROMACS format for the CHARMM force field.[26]

(3) Simulation boxes with a dimension of 4.0 × 4.0 × 4.0 nm were filled with the solvent molecules proportioned to achieve molar fraction compositions of (1) 100% alcohol, (2) 70:30% alcohol/DCM, (3) 50:50% alcohol/DCM, and (4) 55:30:15% alcohol/DCM/water. The alcohols studied included ethanol, propanol, and IPA.

Simulations including only solvent and solvent with polymer were set up with the following conditions: The Velocity−Verlet algorithm was used as the time integrator. Periodic boundary conditions for the simulation boxes were employed with the Verlet cutoff scheme for neighbor searching. Short-range electrostatic interactions were explicitly considered up to a cutoff of 1 nm, and the particle mesh Ewald (PME) method modeled long-range electrostatic interactions.[27] Van der Waals interactions were calculated up to a cutoff of 1 nm.

(4) In preparation for the simulations, the solvent boxes underwent three equilibration stages: (1) a micro-canonical ensemble equilibration over 0.5 ns (NVE), (2) a canonical ensemble equilibration over 1 ns (NVT), (3) and an isothermal−isobaric equilibration over 1 ns (NPT) using a time step of 1 fs/step. The solvent compressibility values used to perform the NPT simulations were: 10.0×10^{-5} bar^{-1} for IPA, 9.0×10^{-5} bar^{-1} for propanol, 11.2×10^{-5} bar^{-1} for ethanol, and 9.9×10^{-5} bar^{-1} for DCM. The compressibility values for mixtures of two solvents were calculated by multiplying the compressibility by the molar fraction of its corresponding solvent.

The polymer simulations involved eight stages:

(1) The chemical structure resembling HPMC E3 LV (30% methoxyl (M), 10% hydroxypropoxyl (P), 60% hydroxyl (H)) was sketched in HyperChem 8.0.[28] The polymer chain included 20 monomers (537 atoms), and the composition is described in Table 1.

(2) An energy minimization of the polymer chain was performed, with the Polak−Ribiére (conjugate-gradient) algorithm, using a root-mean-square (RMS) gradient of 1.0×10^{-2} kcal $Å^{-1}$ mol^{-1} as convergence conditions.

(3) The HPMC structure was submitted to the online topology building tool SwissParam[26] to obtain topology files in GROMACS format for the CHARMM force field.

(4) Next, the polymer chain was solvated using the previously equilibrated solvent boxes. The solvated system included ∼15 000 solvent molecules in cubic boxes with edges of up to 12.0 nm.

(5) The solvated-polymer system was first minimized using a steepest descent algorithm (0.01 fs/step), and the minimization was stopped when the maximum force was less than 100.0 kJ mol^{-1} nm^{-1}.

(6) Second, a NVT equilibration was performed for 5 ns (1 fs/step) using the v-rescale thermostat, at a reference

DOI: 10.1021/acs.molpharmaceut.8b00324
Mol. Pharmaceutics 2018, 15, 3236−3251

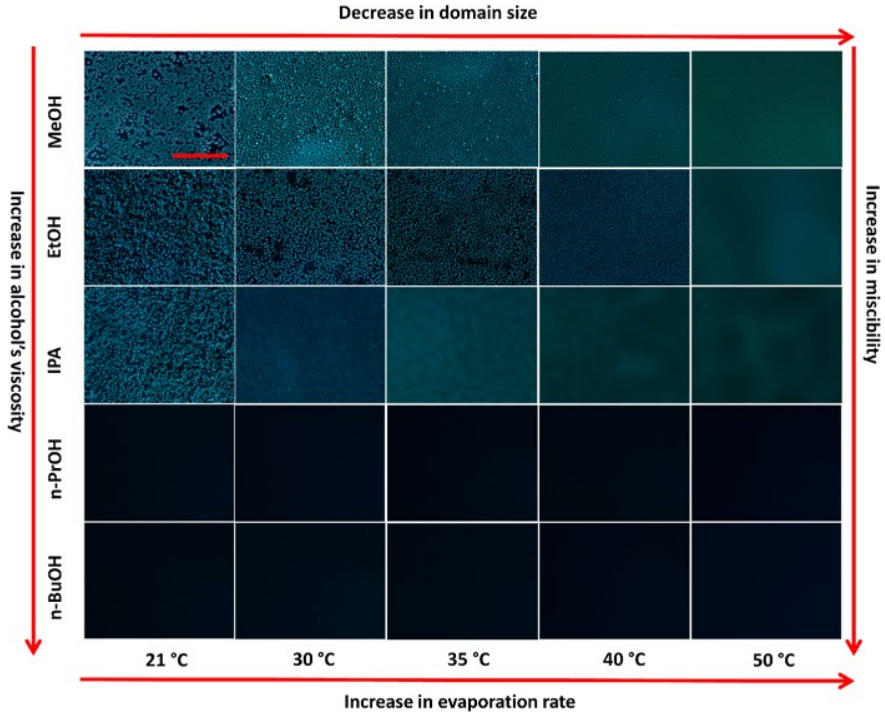

Figure 2. FL optical micrographs of ITZ/HPMC spin-coated films, prepared at different temperatures and 50% RH, using different alkyl alcohols as a cosolvent (scale bar corresponds to 20 μm).

temperature of 294 K, with a coupling constant (tau-t) of 0.2 ps.

(7) Third, an NPT equilibration was carried out for 5 ns (1 fs/step) using the v-rescale thermostat, at a reference temperature of 294 K, with a coupling constant (tau-t) of 1.0 ps; and the Berendsen barostat at a reference pressure of 1 bar, with a coupling constant (tau-p) of 1.0 ps.

(8) Finally, the production run was performed for 20 ns, at 1 fs/step, recording output to disk every 10 ps, under the isothermal–isobaric (NPT) ensemble, at a reference temperature of 294 K, with a coupling constant (tau-t) of 1.0 ps; and with the Berendsen barostat at a reference pressure of 1 bar, with a coupling constant (tau-p) of 1.0 ps.

The trajectories from the first NPT equilibration and the production run were analyzed, and variations in the radius of gyration (R_g) and radial distribution functions (RDF) in the presence of various solvent compositions are reported. The RDF is computed between all the atoms of the polymer and all the atoms of the solvent molecules.

Following the same equilibration and production stage steps, a different set of simulations were performed, using four polymer chains and alcohol/DCM or alcohol/DCM/water compositions. The purpose of this set of simulations was to determine the effect of water on the dynamics of the polymer chains.

4. RESULTS

The phase behavior of ITZ/HPMC film produced via spin coating from a 50:50 MeOH/DCM solvent mixture has been reported previously, with phase separation attributed to the presence of water in the system.[12,13] Herein, we examine the effect of the alkyl alcohol chain length on the polymer conformation and as a consequence on the phase behavior of the produced films.

4.1. Phase Behavior of Films Produced at 50% RH.

FLOM was utilized as an initial screening tool to assess miscibility of the drug/polymer systems based on the distribution of ITZ fluorescence intensity; ITZ is autofluorescent. At room temperature (21 °C ± 0.5) and at 50% RH, films produced using MeOH, EtOH, and IPA cosolvent systems displayed clear phase separation, with regions of high fluorescence intensity indicating the nonuniform distribution of the drug in the films, as shown in Figure 2. In contrast, the use of *n*-PrOH and *n*-BuOH as cosolvents produced miscible drug/polymer films, as inferred from the homogeneous distribution of the fluorescence intensity. Upon temperature increase, the size of the phase separated domains decrease in films spin coated from DCM/MeOH and DCM/EtOH. Films prepared using DCM/IPA showed an absence of discrete domains when prepared above 30 °C; however, the fluorescence intensity distribution was inhomogeneous, with the microstructure being similar to that associated with spinodal decomposition.[13] For films spin coated from DCM/PrOH and DCM/BuOH, the temperature at which films were produced did not impact their phase behavior as assessed by FLOM.

Due to the limited spatial resolution of FLOM imaging, complementary techniques were utilized to enable further investigation of changes in the size of phase separated domains at elevated temperature where the domain sizes are below the diffraction limit of optical microscopy. Thus, TEM was employed as a high-resolution technique to investigate film texture. Bright field (BF) TE microscopy enables phase separated domains in the nanometer range to be detected.[12] Samples exhibiting the clearest evidence of phase separation,

DOI: 10.1021/acs.molpharmaceut.8b00324
Mol. Pharmaceutics 2018, 15, 3236–3251

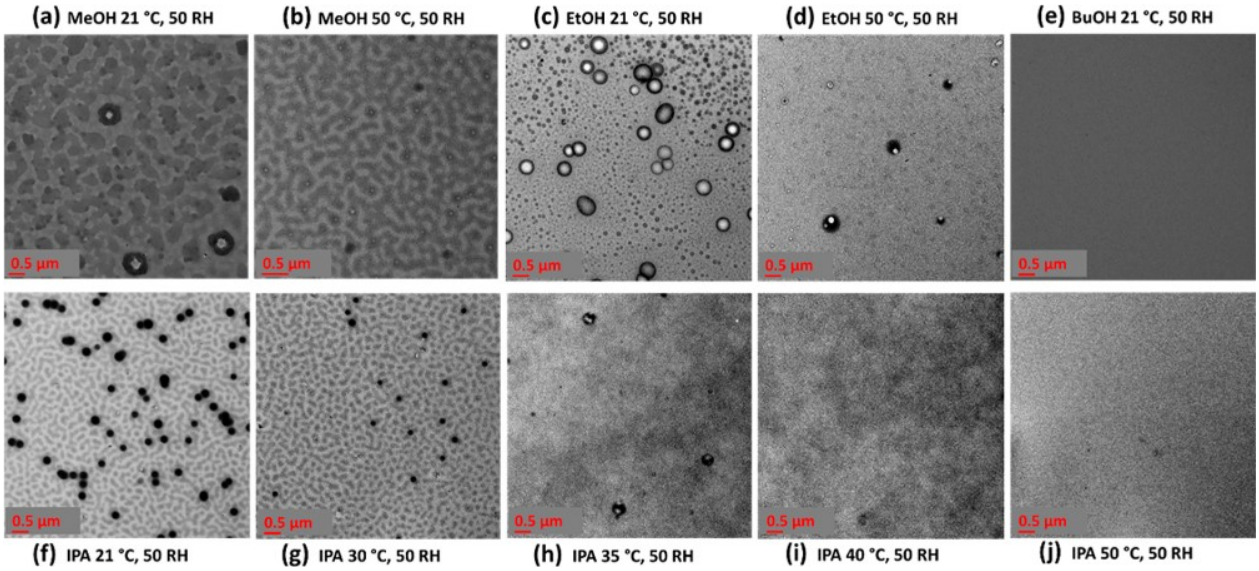

Figure 3. BF TE micrographs of spin-coated films at 50% RH from DCM/MeOH (a) at 21 and (b) at 50 °C, DCM/EtOH (c) at 21 and (d) at 50 °C, DCM/BuOH (e) at 21 °C, and DCM/IPA at (f) 21, (g) 30, (h) 35, (i) 40, and (j) 50 °C.

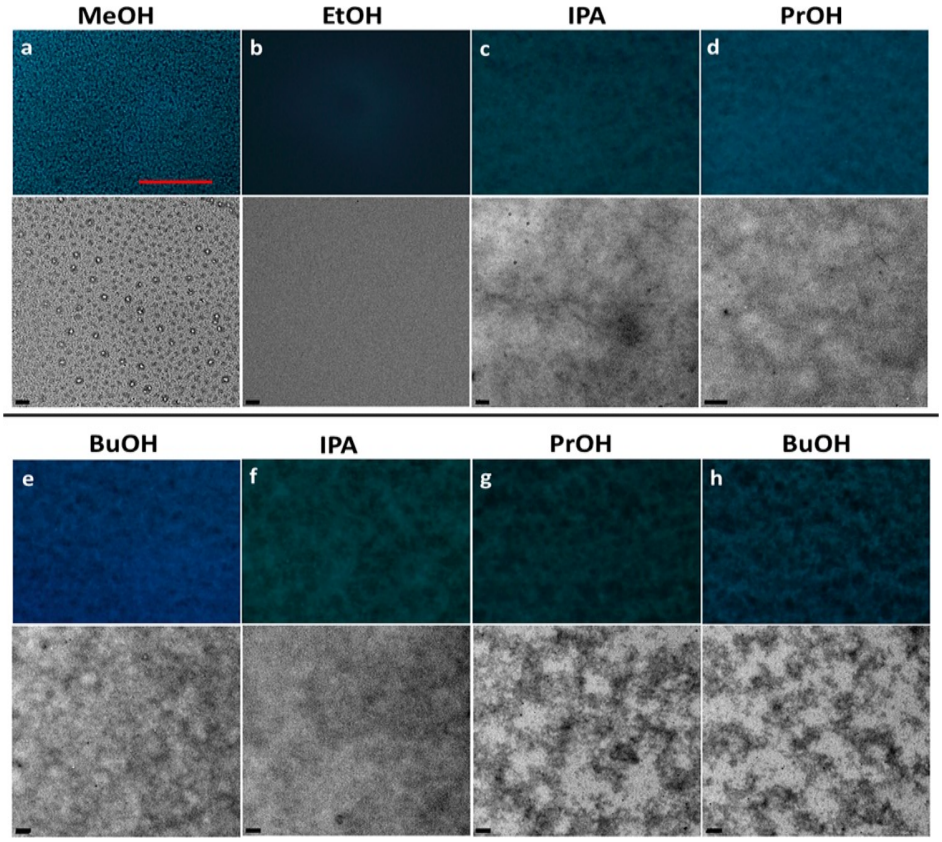

Figure 4. FL optical micrographs and BF TE micrographs of ITZ/HPMC spin-coated films from (a) DCM/MeOH, (b) DCM/EtOH, (c) DCM/IPA, (d) DCM/PrOH, and (e) DCM/BuOH at 21 °C and 20% RH and films spin coated from (f) DCM/IPA, (g) DCM/PrOH, and (h) DCM/BuOH at 21 °C and 7% RH.

based on FLOM imaging, are shown in Figure 3. BF TE micrographs shown in Figure 3a–d illustrate the reduction in size of the discrete ITZ phase separated domains with an increase in temperature for samples spin coated from DCM/MeOH and DCM/EtOH. The presence of a second form of phase separation in the continuous phase of films produced at 21 and 50 °C from DCM/MeOH system is also apparent; this was not seen in the DCM/EtOH films where only discrete domains were observed (Figures 3c,d). The use of DCM/BuOH at 21 °C led to homogeneous films, (Figure 3e), confirming miscibility, in spite of the high RH conditions employed (50% RH). Films produced from the IPA-containing

DOI: 10.1021/acs.molpharmaceut.8b00324
Mol. Pharmaceutics 2018, 15, 3236–3251

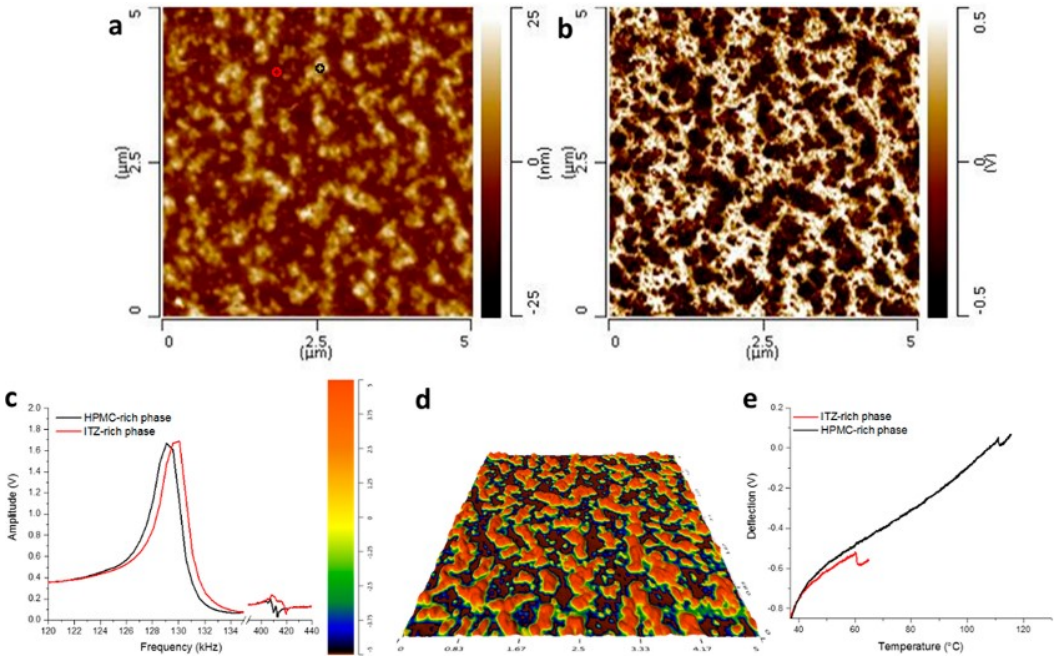

Figure 5. AFM topographic image produced using contact mode (a), LCR amplitude image at 130 kHz (b), along with the nanomechanical spectra collected for ITZ and HPMC (c), 3D representation (d), and localized (nano-) thermal analysis (e) obtained from ITZ/HPMC films spin coated from IPA/DCM at 21 °C and 20% RH in Figure 4c, where the red and black marks are located.

system at various temperatures are displayed in Figure 3f–j. Films produced at 21 and 30 °C displayed evidence of both discrete domains and a finely dispersed microstructure, with the discrete domains being smaller when spin coating was carried out at 30 °C. Upon increasing the evaporation temperature to 35 °C, fewer discrete domains were observed with a change in the microstructure of the background. Increasing the evaporation temperature to 50 °C eliminated the discrete domains, and films appeared more homogeneous than those produced at lower temperatures.

To investigate whether the reduction in discrete domain size at elevated temperature is due to a temperature or an evaporation rate effect, a second set of films was produced at a lower spinning speed (Figure SI.1). Films produced at a lower spinning rate exhibited larger domain sizes for comparable temperatures, suggesting that the reduction in domain size observed at high temperatures is mainly due to an increase in evaporation rate.

4.2. Phase Behavior of Films Produced at 20% RH. Because the phase separation observed for the ITZ/HPMC system spin coated from DCM/MeOH is attributed to water, absorbed from the atmosphere during spin coating.[13] It was of interest to explore phase behavior for films prepared from the different alcohol cosolvent systems at a lower environmental RH (20%). Films produced from DCM/MeOH solution, at 21 °C and 20% RH (Figure 4a), were found to be phase separated in good agreement with previous observations.[13] In contrast, when EtOH was used as the cosolvent, FLOM and BF TEM images indicated that a miscible system is produced (Figure 4b). Films from IPA were heterogeneous but lacked discrete domains (Figure 4c). Somewhat surprisingly, PrOH and BuOH cosolvent systems at low RH led to phase separated films (Figure 4d,e). Further reduction of the environmental humidity to 7% RH did not produce miscible films in the case of DCM/IPA, DCM/PrOH, and DCM/BuOH systems as shown in Figure 4f–h, respectively. These results were counterintuitive based on observations that miscible films were produced from MeOH/DCM at 7% RH.[13] It should be highlighted that EtOH, IPA, PrOH, and BuOH are capable of forming an azeotropic mixture with water while MeOH cannot. This indicates that the 95.5/4.5% EtOH:H_2O system will behave as a one-component system with a boiling point of 78.2 °C.[29] Similarly, the 87.9:12.1% IPA/H_2O system will evaporate at 80.4 °C as a one-component system. Thus, when 20% RH was employed the water content, acquired from the environment might have been reduced to or below the azeotropic composition compared to the higher amount of moisture absorbed when spin coating was carried out at 50% RH. PrOH and BuOH can form 71.7 and 55.5% azeotropes with water, respectively.[29] Thus, they can evaporate as a single-component solvent even with a larger amount of water, which could explain the miscibility of the films produced from those two systems at 50% RH.

4.3. Investigation of Compositional Variation in the Phase Separated Films. Purohit and Taylor have previously identified the discrete domains as an ITZ-rich phase for a system prepared from DCM/MeOH under uncontrolled humidity conditions.[12] Herein, it was of interest to investigate the composition of the bicontinuous microstructure observed in some of the films. AFM coupled with Lorentz contact resonance (LCR) imaging was employed for this purpose, focusing on films spin coated from the DCM/IPA system at 20% RH. The topographical images in Figure 5a revealed that the film surface was uneven with protruding features in a semicontinuous arrangement. In LCR amplitude imaging, images are collected based on the relative stiffness of components in the spin-coated films upon applying the appropriate drive frequency. As a result, individual components can be selectively highlighted where bright areas will be visible when the contact frequency between the probe and the

DOI: 10.1021/acs.molpharmaceut.8b00324
Mol. Pharmaceutics 2018, 15, 3236–3251

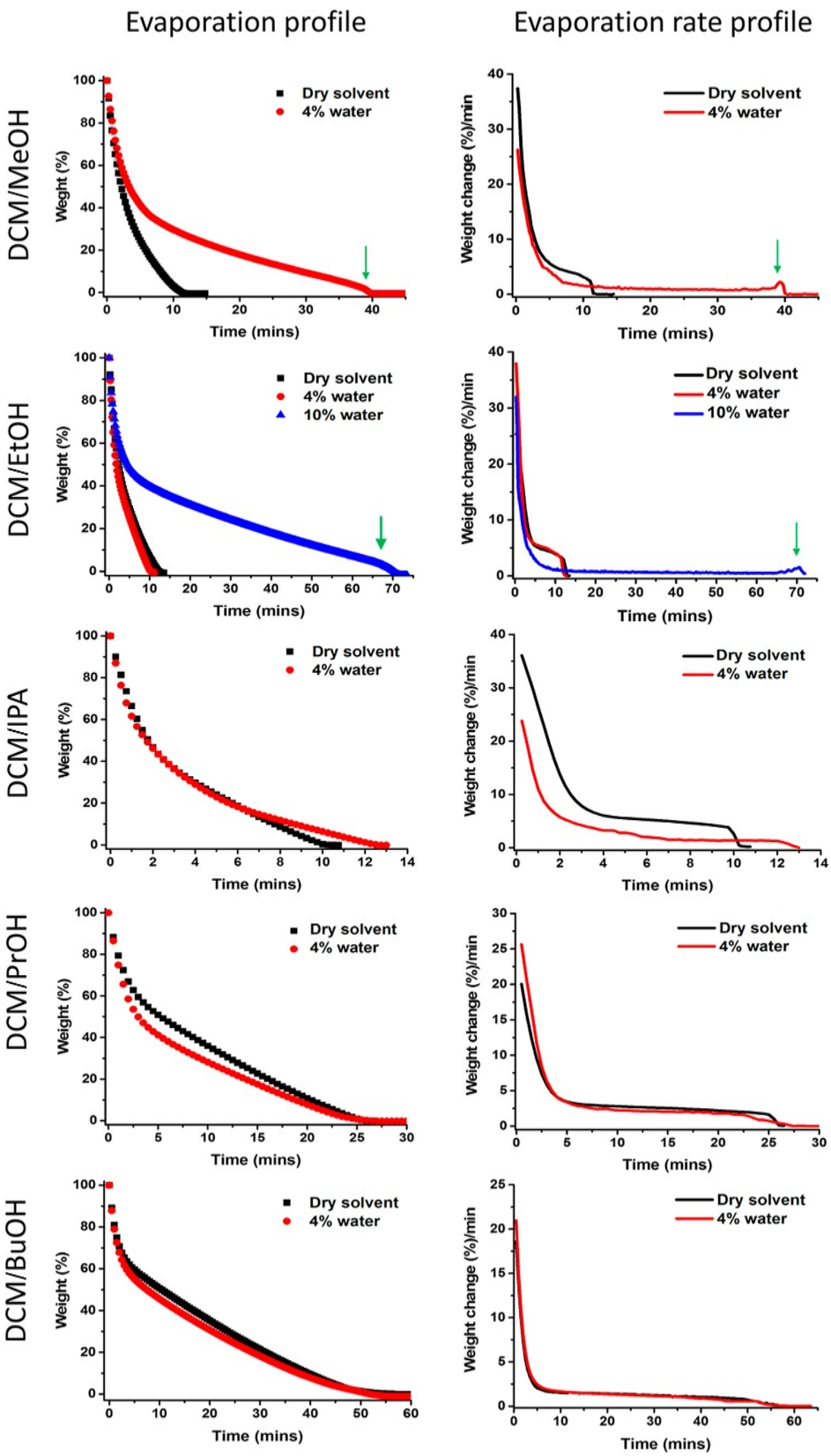

Figure 6. Evaporation profile (weight %) vs time and evaporation rate profile (weight change %/min) vs time of pure solvent mixtures.

scanned area is the same as the applied LCR drive frequency. On the basis of the nanomechanical spectra in Figure 5c, ITZ is stiffer than HPMC, and thus, when the LCR drive frequency is set to 130 kHz, ITZ-rich regions appeared bright in the LCR amplitude image, while HPMC-rich regions are correspondingly dark (Figure 5b). This indicates that the high features in

DOI: 10.1021/acs.molpharmaceut.8b00324
Mol. Pharmaceutics 2018, 15, 3236−3251

the film, appearing as an orange color in the 3D plot in Figure 5d, correspond to HPMC. These results were confirmed using nanothermal analysis of both bright and dark regions as can be seen in Figure 5e where the softening behavior was investigated. The softening temperature of the high features was ~115 °C, while that of the continuous phase was ~60 °C, consistent with the glass transition values of HPMC and ITZ, respectively.[12]

4.4. Impact of Water on the Evaporation Profile of Various Solvent Systems. To better understand the solvent evaporation process and how it is impacted by the initial solvent composition, the evaporation of solvent systems containing DCM with select alcohols, dry and in the presence of a known amount of water, was monitored gravimetrically as described previously.[8] The evaporation profile of a given cosolvent mixture was found to be highly dependent on the water content as shown in Figure 6. The DCM/MeOH mixture containing 4% water showed the same initial evaporation rate as the dry solvent blend, but subsequently, the evaporation rate was dramatically reduced such that the total evaporation time was extended by a factor of 4. In contrast, the presence of 4% water does not seem to impact the evaporation rate of the DCM/EtOH solvent system, while the addition of 10% water to the mixture resulted in a 7-fold increase in the evaporation time. Biphasic evaporation profiles were observed with dry DCM/MeOH, dry DCM/EtOH, and DCM/EtOH with 4% water with the evaporation rate decreasing with time. More complex evaporation profiles were observed upon the addition of 4% water to the DCM/MeOH and 10% water to the DCM/EtOH systems. Here, there was an initial rapid decrease in the evaporation rate similar to that observed for the dry solvent blends followed by a decreased evaporation rate. A sudden increase in the evaporation rate, in both samples, was observed immediately prior to complete evaporation. For the DCM/IPA solvent system, the addition of 4% water delayed complete evaporation by 2.5 min. However, the shape of the evaporation and evaporation rate profiles were not affected. For DCM/PrOH and DCM/BuOH solvent mixtures, 4% water did not affect the evaporation time compared to their dry counterparts, and the profiles were similar for dry and wet solvents.

4.5. Solubility–Temperature Phase Diagram of ITZ in Alkyl Alcohols. The temperature dependent solubility line of ITZ in alkyl alcohols was determined using clear and cloud point measurements for suspensions with different initial compositions. Figure SI.2a shows the "clear point" solubility line. The clear point is defined as the temperature at which all the crystals are dissolved upon heating an ITZ crystalline suspension. Figure SI.2b shows the "cloud point" solubility line. The cloud point is defined as the temperature at which turbidity appears once the previously heated solution is cooled down.

Since the starting material is crystalline ITZ, the clear point corresponds to the crystalline solubility of the drug. Crystalline ITZ shows the lowest solubility in IPA and the highest solubility in MeOH. The properties of the particulate species following cooling of the solution were investigated using PXRD and DSC (Figures SI.3 and SI.4). The PXRD results indicated that the particulates formed during cooling were predominantly amorphous with some Bragg peaks characteristic of crystalline ITZ being present for samples from MeOH, EtOH, IPA, and PrOH; these were absent in the BuOH precipitate. In agreement with these data, DSC thermograms (reversing heat flow) for precipitates from lower alcohols exhibited a very weak glass transition in addition to a melting endotherm characteristic for crystalline ITZ.[30] In contrast, the precipitate from the higher alcohols exhibited thermal events characteristic of glassy ITZ: a glass transition (T_g) followed by two liquid crystalline transitions (T_{LC1} and T_{LC2}).[31] The phase separation concentration during cooling is quite similar for all the alcohols tested except for IPA, where the solubility in this alcohol is much lower than for the other systems evaluated.

4.6. Investigation into the Polymeric Monomer/Agglomerates Size. The sizes of HPMC species in stock solutions of different DCM/alcohols blends, before and after partial evaporation, are shown in Figure 7. Acknowledging that

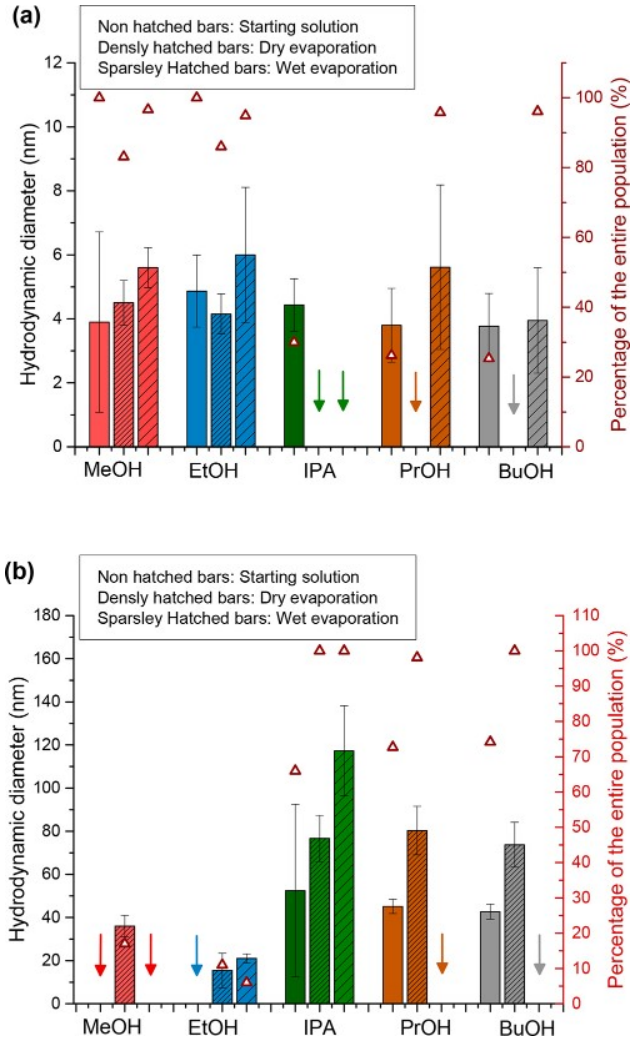

Figure 7. Mean hydrodynamic diameter of (a) the molecules and (b) aggregates of HPMC alcohol/DCM initial solutions and solutions partially evaporated either under dry conditions or at 50% RH. The open triangles and second *y*-axis show the % intensity for the various species.

the actual size is challenging to measure and that only a comparison of the hydrodynamic diameters is carried out herein, values below 10 nm are assigned to polymer molecules (individual chains) and are shown in Figure 7a, while species above 10 nm are considered to indicate aggregates, and results are summarized in Figure 7b. The mean hydrodynamic

DOI: 10.1021/acs.molpharmaceut.8b00324
Mol. Pharmaceutics 2018, 15, 3236−3251

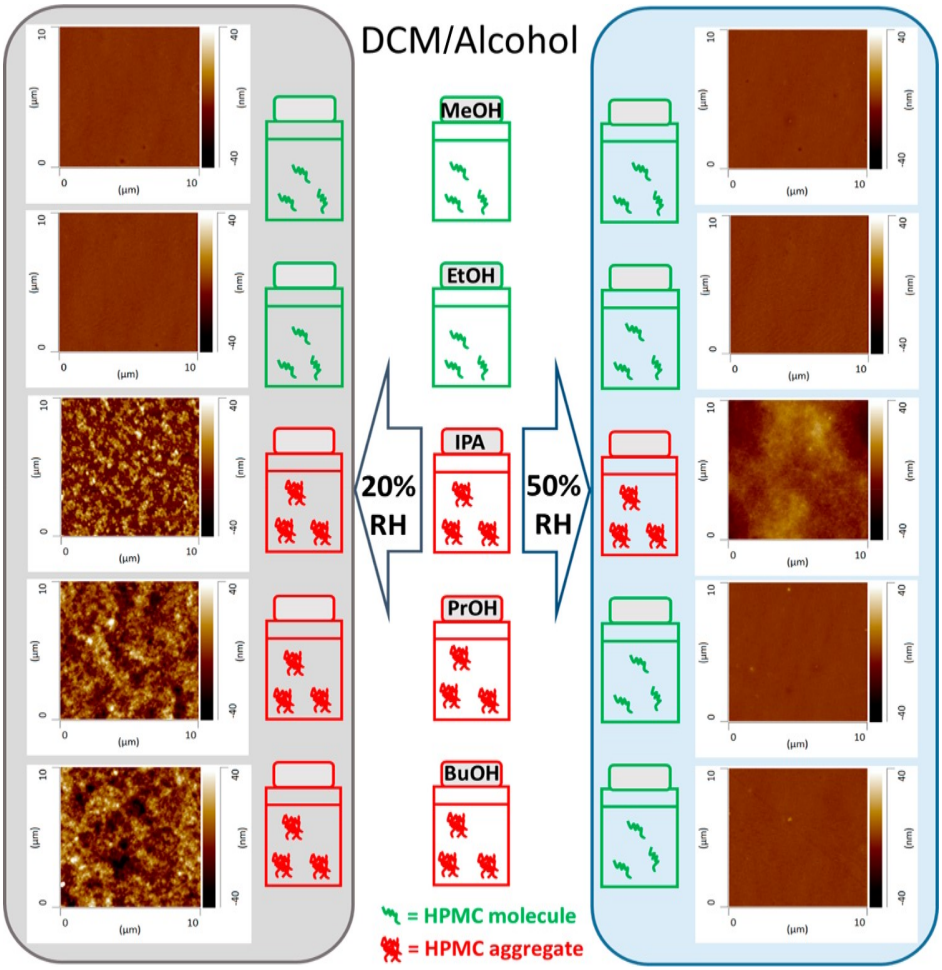

Figure 8. Schematic illustration of the correlation between the state of HPMC (individual molecule vs aggregate) in the initial stock solution and upon evaporation under dry (20% RH) and wet (50% RH) conditions, according to DLS data, and the texture of the HPMC spin-coated films investigated using AFM.

diameter of HPMC molecules measured in the initial dry stock solutions before evaporation was 4−5 nm. There were no other peaks observed in the MeOH and EtOH solutions with DCM. However, a second population with a mean hydrodynamic diameter higher than 40 nm was observed in DCM solutions with the other alcohols indicating that HPMC aggregates are also present in these systems. Following partial evaporation under dry conditions, HPMC started to aggregate in all solutions albeit to different degrees. Furthermore, the population of sub-10 nm hydrodynamic radius species disappeared from IPA, PrOH, and BuOH solutions (green, brown, and gray arrows, respectively, in Figure 7a). Both molecules below 10 nm (Figure 7a) and some aggregates (Figure 7b) were observed in the MeOH and EtOH solutions evaporated under dry conditions. Notably, the percentage of aggregated HPMC in MeOH and EtOH solution upon evaporation under dry conditions was very small (17 ± 4 and 11 ± 5%, respectively) with most of the polymer present as discrete chains.

In contrast, when solutions were evaporated at 50% RH, IPA was the only alcohol where evaporation induced substantial aggregation of HPMC. A few small aggregates (~20 nm, representing 6 ± 4% of the entire population) were observed in the solution of HPMC in EtOH evaporated at 50% RH. Interestingly, in PrOH and BuOH mixtures with DCM, no aggregation occurred upon evaporation at 50% RH. Rather, the aggregates observed in the original solutions of DCM/PrOH and DCM/BuOH disappeared (brown and gray arrows, respectively).

AFM investigation of the topography of the spin-coated HPMC films from various cosolvent systems under dry and wet conditions (Figure 8) could be rationalized by considering the data obtained from the DLS study. Flat films with a smooth surface were produced when the polymer presents as individual chains (molecules) including films spin coated from MeOH and EtOH under dry and wet conditions and from PrOH and BuOH under wet conditions. In contrast, rough films with irregular, corrugated surface topography, were produced when the solution contained polymer aggregates including films produced from IPA under dry and wet conditions and from PrOH and BuOH under dry conditions.

4.7. Solubility Parameters Calculations. The solubility parameters of Methocel have been reported previously by Archer (1992).[18] The reported values for the E3 grade employed in this study were, δ_{di} = 17.4 MPa$^{1/2}$, δ_{pi} = 14.9 MPa$^{1/2}$, and δ_{hi} = 19.3 MPa$^{1/2}$. In addition, the radius of interaction (R_0) was found to be 7.6 MPa$^{1/2}$. The distance between the total solubility parameters of the polymer and various alcohols employed in this study is displayed in Figure 9a. The distances between the three-dimensional solubility

DOI: 10.1021/acs.molpharmaceut.8b00324
Mol. Pharmaceutics 2018, 15, 3236−3251

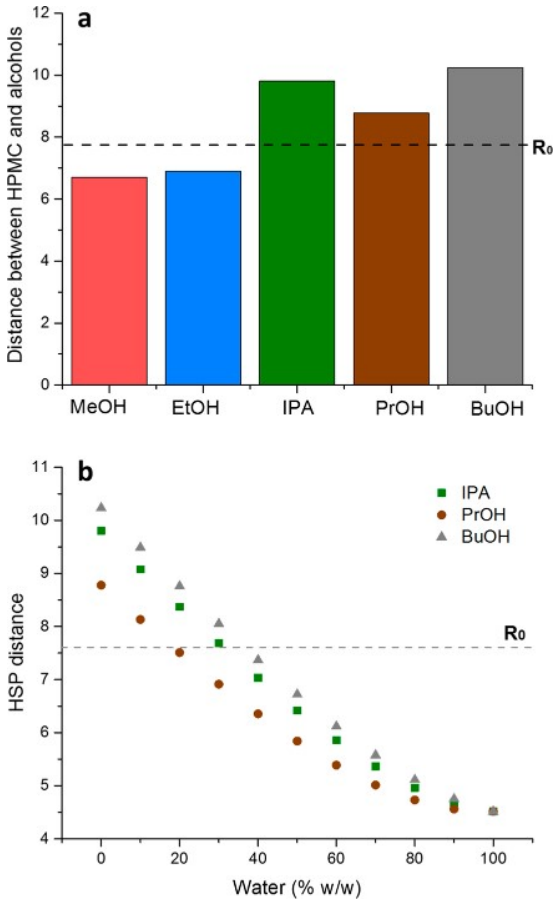

Figure 9. (a) Hansen solubility parameters (HSP) distance of HPMC with various alcohols. The dashed line represents the interaction radius of HPMC. (b) The change in HSP distance of HPMC with various alcohols upon the addition of water. The dashed line represents the interaction radius of HPMC.

parameters center of HPMC and the total solubility parameters of MeOH and EtOH were less than the interaction radius of HPMC (R_0 represented by the dashed line in Figure 9a). In contrast, the distances between the three-dimensional solubility parameters center of HPMC and IPA, PrOH, and BuOH were higher than the reported interaction radius (R_0) of HPMC. These observations point toward the decrease in HPMC solubility with an increase in alcohol chain length. Nonetheless, it should be highlighted that the term solubility parameter does not adequately represent the predictive solubility of the system. In addition, the assumption that no nonadditive interactions take place between various components of the system may also lead to inaccuracies.[32] However, this approach is useful to provide insight into the miscibility of a polymer with a solvent, clearly indicating a decrease in polymer solubility with increasing alcohol alkyl chain length.

The addition of water resulted in a decrease in the HSP distance in the case of higher alcohols as can be inferred from Figure 9b. Thus, the polymer is expected to be more soluble in alcohols containing water.

4.8. Molecular Dynamics Simulations. The statistical analysis of the MD trajectories produced in this study were based on calculations of the radius of gyration, R_g: a quantity commonly used in polymer physics to evaluate the structure and dimensions of chain-like materials. For a molecular system containing N particles, at any step of the trajectory, R_g is defined as

$$R_g^2 \equiv \frac{\sum_i^N m_i(\vec{r}_i - \vec{r}_{COM})^2}{\sum_i^N m_i} \quad (4)$$

Average values of R_g along production trajectories are useful. Meaningful details emerged by performing a full statistical analysis on R_g of the polymer. The summary is presented on Figure 10. In all cases, the lowest R_g averages are found at compositions that mix half alcohol and half DCM. In contrast, the highest averages are found in pure PrOH and IPA, while for EtOH, the system peaks at an alcohol proportion of 70%. The effect of increasing the proportion of the alcohol on the conformation of the polymer is more pronounced in the case of IPA than in the case of PrOH, and mixed results are found for EtOH. Roughly, R_g tends to be larger when the proportion of alcohol in the solvent is greater, indicating that a more extended conformation of HPMC may be favored in the presence of alcohols.

Sampling can be challenging in polymer simulations. Therefore, the barriers of the polymer backbone torsions were explored to estimate the height of relevant features of the conformational energy surface of the polymer. The torsional angle C2−C1−O1−C4 was rigidly scanned to explore the conformational freedom of the backbone (see Supporting Information). These torsions are expected to be a more significant restraint than those involving the side chains. This is mainly because the size of the side chain substituents is small

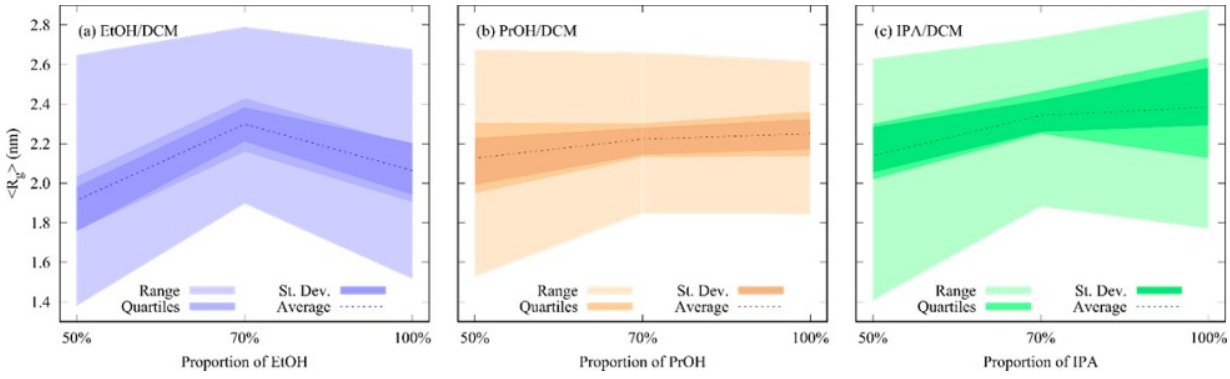

Figure 10. Radius of gyration, $\langle R_g \rangle$, for HPMC in the presence of different alcohol/DCM compositions during the 20 ns NPT production stage. The average, range, standard deviation, and quartiles are shown.

DOI: 10.1021/acs.molpharmaceut.8b00324
Mol. Pharmaceutics 2018, 15, 3236−3251

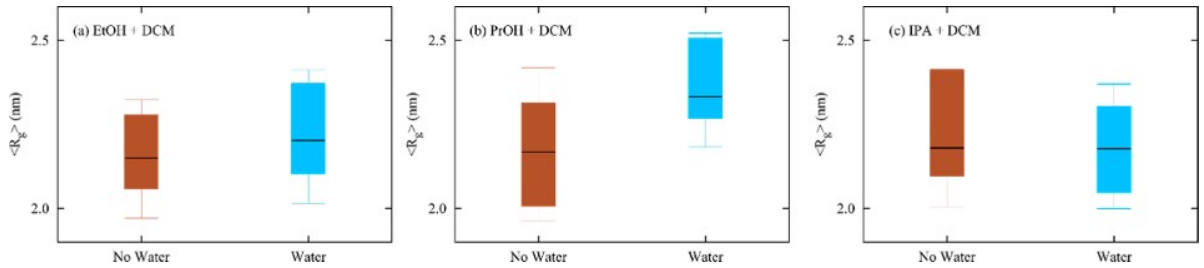

Figure 11. Average radius of gyration, $\langle R_g \rangle$, for four chains of HPMC in the presence (cyan color) and absence (brown color) of water in (a) EtOH, (b) PrOH, and (c) IPA. The black horizontal line corresponds to the arithmetic mean; the candlesticks are centered on the median and represent the standard deviation; the whisker bars show the lower and higher quartiles.

compared to that of the full polymer chain. On average, the estimated energy barrier for the backbone torsion of the substituted-HPMC model is approximately 7 kcal/mol. Considering that the temperature of simulation is around 300 K, such torsions are moderately weak and may have limited impact in conformational sampling.

To analyze the effect of water in the solvent, a comparison was carried out between simulations of four polymer chains with and without water. The results are summarized in Figure 11. Water appears to have a different effect on the R_g of HPMC depending on the type of alcohol present in the solvent. The polymer clearly expands in PrOH, while the R_g shows a limited increase in EtOH, and it remains almost invariant in the case of IPA.

In addition, radial distribution functions (RDF) were determined between all of the atom types of the polymer chains and all of the atom types of the solvent molecules. The RDF represents the probability of finding two sets of atoms at a certain distance. Figure 12 shows the RDF for HPMC/alcohol and HPMC/DCM for different alcohol/DCM mixtures. There are two solvation layers around the HPMC polymer chain, one at approximately 0.55 nm and one at 0.95 nm. Interestingly, for 70:30% alcohol/DCM mixtures, the probability of finding DCM or alcohol near the polymer chain is the same (blue lines). However, when the proportion of DCM increases to 50%, the probability of finding DCM close to the polymer is reduced, and the probability of finding alcohol near the polymer is increased (red lines).

Figure 13 shows the RDF between HPMC and solvent for systems containing four polymer chains in the presence of 55:30:15% alcohol/DCM/water mixtures. The addition of water to the systems causes the creation of two water shells surrounding the polymer chain, one at approximately 0.41 nm and one at 0.78 nm (black line). The probability of finding water close to the polymer is higher than the probability of finding alcohol or DCM molecules. Systems with PrOH and IPA alcohols exhibited a higher probability of finding water close to the polymer than the EtOH system.

5. DISCUSSION

The ITZ/HPMC system has been reported to undergo phase separation when spin coated and spray dried from a DCM/MeOH solvent mixture.[12,13] A recent comprehensive investigation of this system revealed that phase separation was driven by the presence of water, either acquired from the environment or present in the solvent system. Herein, we have further studied the role of water, expanding the study to evaluate solvent characteristics, in particular, higher alcohols,

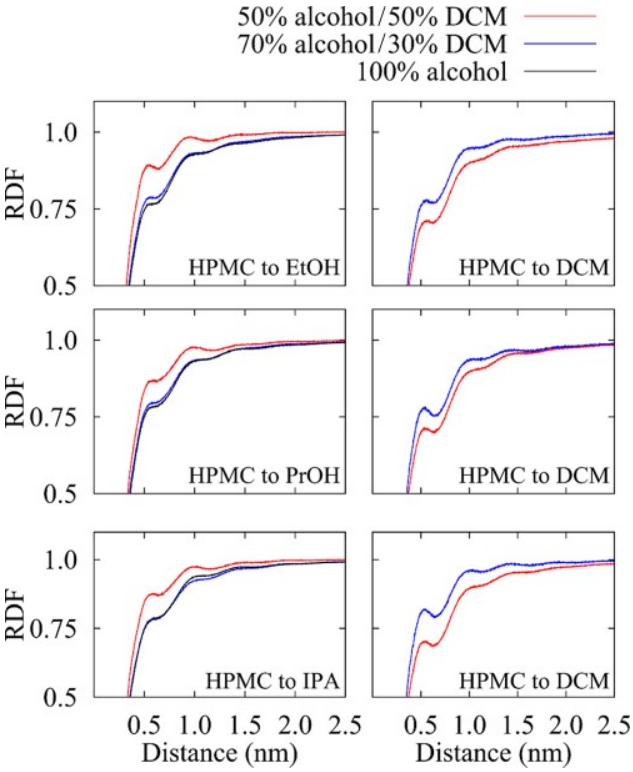

Figure 12. Radial distribution function for HPMC with the solvent in the presence of different alcohol/DCM mixtures.

and polymer conformation on the phase behavior of the ITZ/HPMC system.

Solvent selection for ASD formation is often empirical and typically driven by the need to find a common solvent/solvent mixture for all the ASD components. However, solvent properties can impact the properties and microstructure of the resultant ASD differently. Findings from this study indicate that small amounts of water, present as a contaminant in the solvent system, can be a double-edged sword in terms of impact on miscibility. The presence of water in the solvent system during ASD fabrication has been reported to lead to phase separation for a number of systems.[33,34] ITZ/HPMC phase behavior when prepared from the lower alcohol/DCM solvent system followed the expected trend, whereby water led to phase separation and the formation of discrete drug-rich domains. However, the improvement in miscibility induced by water for the higher alcohols solvent systems, as observed herein, is a somewhat surprising observation. These observations are of particular interest for HPMC-based ASDs, since

DOI: 10.1021/acs.molpharmaceut.8b00324
Mol. Pharmaceutics 2018, 15, 3236−3251

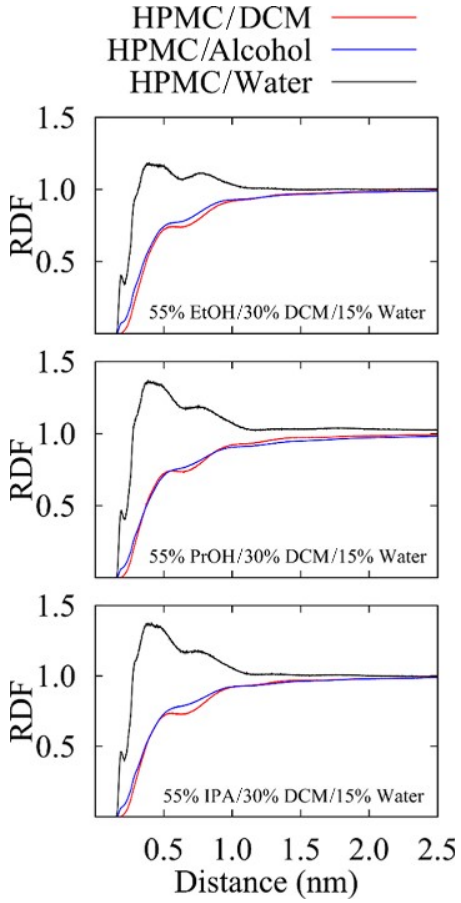

Figure 13. Radial distribution function for HPMC with the solvent for systems with four polymer chains in the presence of 55:30:15% alcohol/DCM/water.

most grades of this polymer are not soluble in single-component organic solvent systems, necessitating the use of multicomponent solvent systems. To facilitate discussion of the phase behavior, the cosolvent alcohols will be categorized into lower alcohols (MeOH and EtOH) and higher alcohols (IPA, PrOH, and BuOH).

When lower alcohols were chosen as cosolvents, dry conditions were necessary to ensure that ITZ and HPMC intimately mixed in the ASD. When the spin coating process was carried out at 21 °C and 50% RH, both solvent systems led to the formation of phase separated domains, which decreased in size with an increase in evaporation rate (Figure 2). When the humidity in the environment was lowered to 20% RH, the EtOH cosolvent system resulted in a miscible ASD, while the DCM/MeOH solvent system resulted in a phase separated ASD. For the latter system, only after reduction of the ambient relative humidity to 7% could a miscible ASD be produced.[13] It is well established that the absorption of water is favored at a higher humidity due to the higher partial pressure of water in the atmosphere.[35] Thus, it is expected that less water will be absorbed during spin coating at 20% RH. For EtOH, at 20% RH, the equilibrium water content is less than 3% by volume, which is close to, but below the azeotropic composition of the EtOH/H_2O binary mixture, which is 95:5% EtOH/H_2O by volume.[29] Given that the system is EtOH-rich relative to the azeotropic composition, evaporation will lead to residual liquid that is rich in EtOH, and the concentration of H_2O will not occur in the solution. Of course, this analysis does not consider the impact of either DCM or the dissolved solutes on the azeotropic composition, and these are unknown factors. In contrast, MeOH does not form an azeotropic system with water. Hence, MeOH is anticipated to evaporate faster than water, leading to an increase in the H_2O concentration in the residual solution. The presence of as little as 1% water in the DCM/MeOH stock solution has been reported to induce phase separation in spray dried ITZ/HPMC solid dispersions due to the poor aqueous solubility of ITZ.[13] Thus, it has to be prepared at very low humidity (7% RH) to ensure that the water content in the solvent system is minimized and that the resultant ASD is miscible.

Support for these suppositions is provided by the solvent evaporation and evaporation rate profiles (Figure 6). For the solvent mixtures, without any dissolved materials, the inclusion of 4% water substantially reduced the evaporation rate of the DCM/MeOH mixture. In contrast, the inclusion of 4% water did not impact the evaporation of the DCM/EtOH solvent mixture (Figure 6). To summarize, both EtOH and MeOH are hygroscopic solvents that are expected to acquire water from the atmosphere during spin coating. For EtOH, which forms an azeotrope with H_2O during solvent evaporation, high initial water contents (>5% by volume) are expected to lead to water concentration, while low initial water contents will result in EtOH concentration. For MeOH systems, H_2O concentration is anticipated during evaporation. Because of the low aqueous solubility of ITZ, phase separation of the drug to form discrete domains is anticipated to occur when water concentration occurs during solvent evaporation and when the evaporation rate is slow. Using this framework, our experimental observations can be largely rationalized.

Higher alcohols and H_2O impacted the phase behavior of the drug/polymer films differently. IPA displayed a unique behavior when used as a cosolvent with DCM. At 20% RH, the spin-coated ITZ/HPMC system was found to display a network-like corrugated structure at all of the investigated temperatures (21−50 °C). The fact that the high features in the AFM topographical images are HPMC-rich (Figure 5), coupled with the aggregation of HPMC in the IPA-containing solvent system both in solution state (Figure 7a,b) or in the deposited film (Figure 8) suggests that the observed phase separation at 20% RH is due to the incompatibility of the polymer with the solvent system. At higher relative humidity and lower temperatures, discrete, spherical domains embedded in an inhomogeneous background are observed. Not only is the polymer poorly soluble in IPA, but ITZ also shows the lowest solubility in this alcohol (Figure SI.2a,b). The absorption of water will further reduce the drug solubility; hence, the discrete domains are likely to consist of a drug-rich phase. Thus, for IPA cosolvent systems, the phase behavior is extremely complex with both low drug and polymer solubility coming into play, depending on the water content of the system.

PrOH and BuOH impacted ITZ/HPMC phase behavior similarly in the cosolvent system. Both solvents can form an azeotrope with water at relatively high contents of water (71.7 and 55.5% PrOH and BuOH with water, respectively).[29] Hence, during evaporation, the system will concentrate with respect to the alcohol and not H_2O. This is likely why the presence of water did not markedly impact the evaporation time (Figure 6). Interestingly, the presence of water was necessary to ensure solubilization of HPMC in these higher

DOI: 10.1021/acs.molpharmaceut.8b00324
Mol. Pharmaceutics 2018, 15, 3236−3251

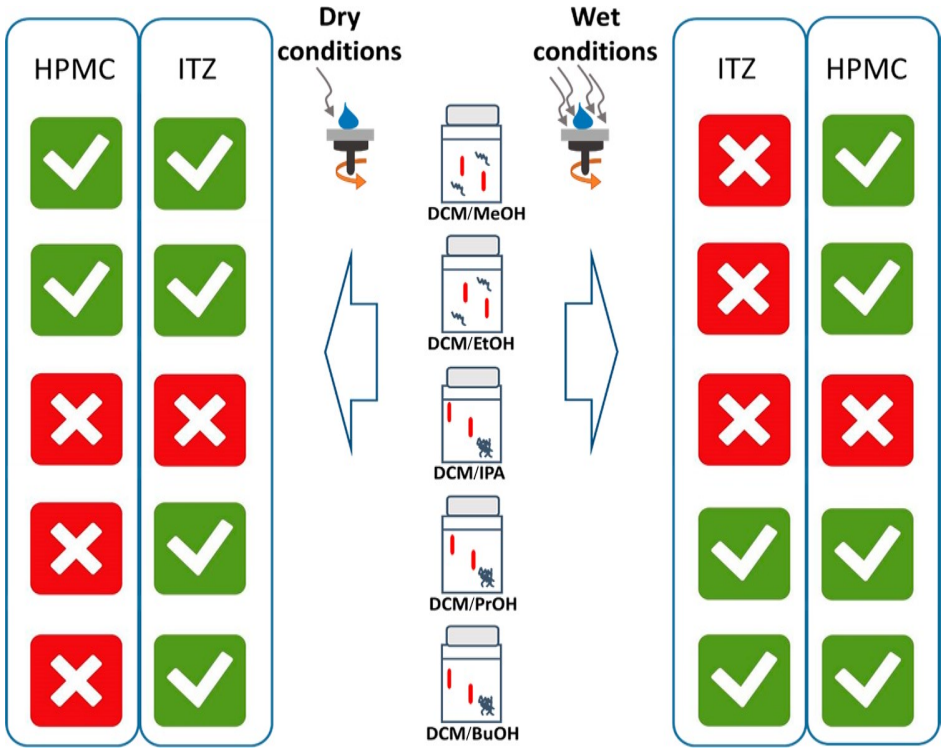

Figure 14. Schematic representation of the impact of water on the phase behavior of the ITZ−HPMC solid dispersion. Green checks indicate the compatibility of the component with the solvent, while red crosses indicate incompatibility of the component with the solvent.

alcohols systems, based on the formation of phase separated films when produced at low RH as well as the polymer aggregation during evaporation under dry conditions as illustrated by DLS results (Figure 7) and film texture investigated using AFM (Figure 8). Hansen sphere theory suggests that the longer the alcohol chain, the lower the miscibility of the polymer in that alcohol, and the miscibility also decreases with branching as in the case of IPA (Figure 9a). The analysis also indicates that the addition of water increases the miscibility of the polymer in the higher alcohols (Figure 9b). The impact of higher alcohol viscosity on the phase behavior of this system also needs to be considered. The viscosity of alkyl alcohols increases with an increase in alkyl chain length with the following literature values reported at 20 °C: MeOH = 0.55 cP,[36] EtOH = 1.19 cP,[37] IPA = 2.27 cP,[36] PrOH = 2.2 cP,[36] and BuOH = 2.95 cP.[36] It is generally accepted that an increase in viscosity results in a decrease in molecular diffusivity, which in turn decreases the nucleation rate of a new phase.[38] Thus, higher alcohols are expected to reduce the diffusion of solute molecules to form drug-rich domains.

Overall observations are summarized in Figure 14. Although all initial solutions were visually transparent suggesting complete solubility of solid components in the solvent mixture, the polymer was found to exist as aggregates when higher alcohols were used as a cosolvent (Figures 7a,b). This solvophobic behavior of HPMC in higher alcohols is responsible for the production of irregular HPMC films under dry conditions (Figure 8). Luo and Eisenberg have reported that the aggregate size for a block copolymer depends on solvent composition for a complex organic solvent mixture.[39]

Our data suggests that HPMC needs to exist as discrete molecules in the extended conformation in the solvent system in order to produce an intimately mixed ASD. In addition, the discrete domains and spinodal decomposition seem to be induced by incompatibility of the drug with water present in the solvent system, while the network-like corrugations are likely induced by solvent incompatibility with HPMC. It is anticipated that the presence of water enables the polymer to remain as a single chain in the preferred extended conformation in the higher alcohols. It has been reported that extended polymer conformations are important to promote interaction with drug molecules and prevent drug crystallization.[40] The impact of solvent on the preferred conformation of hydrophilic polymers such as polyethylene glycols (PEG) has been investigated,[41] whereby three molecules of water were found to be required for hydration of each ethylene oxide unit in a PEG chain. The influence of hydration shell structure on the conformational stability and function of hydrophilic polymers and biomolecules including proteins and DNA has been extensively investigated in the literature.[42] In the present study, MD simulations were useful to determine how variations in the solvent composition influence variables such as the R_g of HPMC and the RDF between polymer and solvent atoms. The R_g values were susceptible to the composition of the solvent mixture, with the lowest R_g values observed for systems with a 50:50% DCM/alcohol composition (Figure 10). The addition of more DCM to the mixture caused a lower probability of finding DCM close to the HPMC chain, and instead, an increased probability of finding alcohol (Figure 12). This is an important phenomenon observed for all of the alcohol/DCM systems, which may imply that during the evaporation process of the alcohol/DCM mixture, the solvation shell around the polymer will constantly

DOI: 10.1021/acs.molpharmaceut.8b00324
Mol. Pharmaceutics 2018, 15, 3236−3251

vary depending on the concentration of both solvents. These changes in the solvent composition can subsequently cause variation in the R_g of the polymer. Therefore, the miscibility results shown in Figure 8 will not only depend on the polymer conformation in the initial 50:50 mixture but also on how the polymer conformation changes due to variations in solvent composition during the evaporation process.

Additionally, to determine the effect of the relative humidity in the properties of the HPMC chain, simulations were conducted for 55:30:15% alcohol/DCM/water mixtures. The RDF between HPMC and solvent for these systems (Figure 13) shows that the first layer of solvent surrounding the polymer is predominantly formed by water molecules. Thus, there is a higher probability of finding water than DCM or alcohol within 1 nm of the polymer. This suggests that water will solvate the HPMC polymer chains for DCM/alcohol mixtures that tend to absorb water under high relative humidity. That solvation by water molecules appeared to increase the R_g for HPMC in the presence of PrOH/DCM/water mixtures (Figure 11), in agreement with the results presented in Figure 8 showing the change in film microstructure. These observations around the presence of a water shell around the polymer chain could have important implications for the conformation of the polymer chain as a function of solvent composition and also in the possible phase separation of polymer/drug mixtures.

CONCLUSIONS

Evaluation of the impact of solvent composition and evaporation rate on the phase behavior of spin-coated ASDs revealed that water can be a double-edged sword in terms of drug/polymer miscibility for the ITZ/HPMC system. On the basis of the physicochemical properties of the drug and polymer, in particular, their solubility in the dry and water-containing solvent system, the phase behavior of a specific system can vary even with slight changes in solvent composition. Domain sizes of phase separated regions were also found to decrease with increasing temperature. This study highlights the complex interplay of component properties and formation conditions on the resultant ASD microstructure, and ultimately, these observations may help in the rational design of ASDs produced via solvent evaporation.

ASSOCIATED CONTENT

Supporting Information

The Supporting Information is available free of charge on the ACS Publications website at DOI: 10.1021/acs.molpharmaceut.8b00324.

Fluorescence images of spin-coated drug/polymer films; clear and cloud point data; X-ray diffraction data of precipitates collected from cloud point experiments; DSC thermograms of precipitates collected from cloud point experiments; torsional energy profiles for HPMC dimers used in modeling; range of torsional energies for various HPMC dimers (PDF)

AUTHOR INFORMATION

Corresponding Author

*E-mail: lstaylor@purdue.edu.

ORCID

Lyudmila V. Slipchenko: 0000-0002-0445-2990

Lynne S. Taylor: 0000-0002-4568-6021

Present Address

§Carlos H. Borca, School of Chemistry and Biochemistry, College of Sciences, Georgia Institute of Technology, 901 Atlantic Drive, Atlanta, Georgia 30332, United States

Notes

The authors declare no competing financial interest.

ACKNOWLEDGMENTS

We are grateful to the National Institute for Pharmaceutical Technology and Education (NIPTE) and the U.S. Food and Drug Administration (FDA) for providing funds for this research. This study was funded by the FDA Grant to NIPTE titled "The Critical Path Manufacturing Sector Research Initiative (U01)"; Grant# 5U01FD004275. The Pharmaceutical Research and Manufacturers of America (PhRMA) Foundation is acknowledged for a postdoctoral fellowship granted to NM. We also express our gratitude for funding provided by a Graduate Student Fellowship Award from the American Association of Pharmaceutical Scientists (AAPS), the McKeehan Graduate Fellowship in Pharmacy, and the Migliaccio/Pfizer Graduate Fellowship in Pharmaceutical Sciences, awarded to LM. This research was supported in part through computational resources provided by Information Technology at Purdue University.

REFERENCES

(1) Simonelli, A. P.; Mehta, S. C.; Higuchi, W. I. Dissolution rates of high energy sulfathiazole-povidone coprecipitates II: Characterization of form of drug controlling its dissolution rate via solubility studies. *J. Pharm. Sci.* **1976**, *65* (3), 355−361.

(2) Rumondor, A. C. F.; Stanford, L. A.; Taylor, L. S. Effects of Polymer Type and Storage Relative Humidity on the Kinetics of Felodipine Crystallization from Amorphous Solid Dispersions. *Pharm. Res.* **2009**, *26* (12), 2599−2606.

(3) Caron, V.; Hu, Y.; Tajber, L.; Erxleben, A.; Corrigan, O. I.; McArdle, P.; Healy, A. M. Amorphous Solid Dispersions of Sulfonamide/Soluplus (R) and Sulfonamide/PVP Prepared by Ball Milling. *AAPS PharmSciTech* **2013**, *14* (1), 464−474.

(4) Sun, Y.; Tao, J.; Zhang, G. G. Z.; Yu, L. A. Solubilities of Crystalline Drugs in Polymers: An Improved Analytical Method and Comparison of Solubilities of Indomethacin and Nifedipine in PVP, PVP/VA, and PVAc. *J. Pharm. Sci.* **2010**, *99* (9), 4023−4031.

(5) Serajuddin, A. T. M. Solid dispersion of poorly water-soluble drugs: Early promises, subsequent problems, and recent breakthroughs. *J. Pharm. Sci.* **1999**, *88* (10), 1058−1066.

(6) Zhang, J. X.; Bunker, M.; Parker, A.; Madden-Smith, C. E.; Patel, N.; Roberts, C. J. The Stability of Solid Dispersions of Felodipine in Polyvinylpyrrolidone Characterized by Nanothermal Analysis. *Int. J. Pharm.* **2011**, *414* (1−2), 210−217.

(7) Bank, M.; Leffingwell, J.; Thies, C. Influence of Solvent Upon Compatibility of Polystyrene and Poly(Vinyl Methyl Ether). *Macromolecules* **1971**, *4* (1), 43−46.

(8) Paudel, A.; Van den Mooter, G. Influence of Solvent Composition on the Miscibility and Physical Stability of Naproxen/PVP K 25 Solid Dispersions Prepared by Cosolvent Spray-Drying. *Pharm. Res.* **2012**, *29* (1), 251−270.

(9) Ansari, M. T.; Sunderland, V. B. Solid dispersions of dihydroartemisinin in polyvinylpyrrolidone. *Arch. Pharmacal Res.* **2008**, *31* (3), 390−398.

(10) Al-Obaidi, H.; Brocchini, S.; Buckton, G. Anomalous properties of spray dried solid dispersions. *J. Pharm. Sci.* **2009**, *98* (12), 4724−37.

(11) Wulsten, E.; Kiekens, F.; van Dycke, F.; Voorspoels, J.; Lee, G. Levitated single-droplet drying: Case study with itraconazole dried in binary organic solvent mixtures. *Int. J. Pharm.* **2009**, *378* (1), 116−121.

DOI: 10.1021/acs.molpharmaceut.8b00324
Mol. Pharmaceutics 2018, 15, 3236−3251

(12) Purohit, H. S.; Taylor, L. S. Miscibility of Itraconazole-Hydroxypropyl Methylcellulose Blends: Insights with High Resolution Analytical Methodologies. *Mol. Pharmaceutics* **2015**, *12* (12), 4542−4553.
(13) Mugheirbi, N. A.; Marsac, P. J.; Taylor, L. S. Insights into Water-Induced Phase Separation in Itraconazole-Hydroxypropylmethyl Cellulose Spin Coated and Spray Dried Dispersions. *Mol. Pharmaceutics* **2017**, *14* (12), 4387−4402.
(14) Ricarte, R. G.; Lodge, T. P.; Hillmyer, M. A. Nanoscale Concentration Quantification of Pharmaceutical Actives in Amorphous Polymer Matrices by Electron Energy-Loss Spectroscopy. *Langmuir* **2016**, *32* (29), 7411−7419.
(15) Ricarte, R. G.; Lodge, T. P.; Hillmyer, M. A. Detection of Pharmaceutical Drug Crystallites in Solid Dispersions by Transmission Electron Microscopy. *Mol. Pharmaceutics* **2015**, *12* (3), 983−990.
(16) Mugheirbi, N. A.; O'Connell, P.; Serrano, D. R.; Healy, A. M.; Taylor, L. S.; Tajber, L. A Comparative Study on the Performance of Inert and Functionalized Spheres Coated with Solid Dispersions Made of Two Structurally Related Antifungal Drugs. *Mol. Pharmaceutics* **2017**, *14* (11), 3718−3728.
(17) Hansen, C. M. *The Three Dimensional Solubility Parameter and Solvent Diffusion Coefficient: Their Importance In Surface Coating Formulation*; Danish Technical Press: Copenhagen, 1967.
(18) Archer, W. L. Hansen Solubility Parameters for Selected Cellulose Ether Derivatives and Their Use in the Pharmaceutical-Industry. *Drug Dev. Ind. Pharm.* **1992**, *18* (5), 599−616.
(19) Sorensen, P. Solubility Parameter Concept in Formulation of Liquid Inks. *J. Oil Colour Chem. As* **1967**, *50* (3), 226.
(20) Hansen, C. Hansen Solubility Parameters. https://www.hansen-solubility.com/downloads.php.
(21) Jiang, X.; Wang, Y.; Li, M. Selecting water-alcohol mixed solvent for synthesis of polydopamine nano-spheres using solubility parameter. *Sci. Rep.* **2015**, *4*, 6070.
(22) Van der Spoel, D.; Lindahl, E.; Hess, B.; Groenhof, G.; Mark, A. E.; Berendsen, H. J. C. GROMACS: Fast, flexible, and free. *J. Comput. Chem.* **2005**, *26* (16), 1701−1718.
(23) Brooks, B. R.; Bruccoleri, R. E.; Olafson, B. D.; States, D. J.; Swaminathan, S.; Karplus, M. Charmm - a Program for Macromolecular Energy, Minimization, and Dynamics Calculations. *J. Comput. Chem.* **1983**, *4* (2), 187−217.
(24) MacKerell, A. D.; Banavali, N.; Foloppe, N. Development and current status of the CHARMM force field for nucleic acids. *Biopolymers* **2000**, *56* (4), 257−265.
(25) van der Spoel, D.; Caleman, C.; van Maaren, P. virtualchemistry.org. http://virtualchemistry.org/.
(26) Zoete, V.; Cuendet, M. A.; Grosdidier, A.; Michielin, O. SwissParam: A Fast Force Field Generation Tool for Small Organic Molecules. *J. Comput. Chem.* **2011**, *32* (11), 2359−2368.
(27) Essmann, U.; Perera, L.; Berkowitz, M. L.; Darden, T.; Lee, H.; Pedersen, L. G. A Smooth Particle Mesh Ewald Method. *J. Chem. Phys.* **1995**, *103* (19), 8577−8593.
(28) Froimowitz, M. Hyperchem: A Software Package for Computational Chemistry and Molecular Modeling. *Biotechniques* **1993**, *14* (6), 1010−1013.
(29) Carper, J. The CRC Handbook of Chemistry and Physics. *Libr J.* **1999**, *124* (10), 192.
(30) Mugheirbi, N. A.; Tajber, L. Crystal Habits of Itraconazole Microcrystals: Unusual Isomorphic Intergrowths Induced via Tuning Recrystallization Conditions. *Mol. Pharmaceutics* **2015**, *12* (9), 3468−3478.
(31) Mugheirbi, N. A.; Paluch, K. J.; Tajber, L. Heat induced evaporative antisolvent nanoprecipitation (HIEAN) of itraconazole. *Int. J. Pharm.* **2014**, *471* (1−2), 400−11.
(32) Milliman, H. W.; Boris, D.; Schiraldi, D. A. Experimental Determination of Hansen Solubility Parameters for Select POSS and Polymer Compounds as a Guide to POSS-Polymer Interaction Potentials. *Macromolecules* **2012**, *45* (4), 1931−1936.
(33) Saboo, S.; Taylor, L. S. Water-induced phase separation of miconazole-poly (vinylpyrrolidone-co-vinyl acetate) amorphous solid dispersions: Insights with confocal fluorescence microscopy. *Int. J. Pharm.* **2017**, *529* (1−2), 654−666.
(34) Rumondor, A. C. F.; Wikstrom, H.; Van Eerdenbrugh, B.; Taylor, L. S. Understanding the Tendency of Amorphous Solid Dispersions to Undergo Amorphous-Amorphous Phase Separation in the Presence of Absorbed Moisture. *AAPS PharmSciTech* **2011**, *12* (4), 1209−1219.
(35) De Vrieze, S.; Van Camp, T.; Nelvig, A.; Hagstrom, B.; Westbroek, P.; De Clerck, K. The effect of temperature and humidity on electrospinning. *J. Mater. Sci.* **2009**, *44* (5), 1357−1362.
(36) Fisher Scientific. https://www.fishersci.com/us/en/brands/f/fisher-chemical.html.html.
(37) Kadlec, P.; Henke, S.; Bubnik, Z. Properties of ethanol and ethanol-water solutions - Tables and Equations. *Zuckerindustrie* **2010**, *135* (10), 607−613.
(38) Warren, D. B.; Benameur, H.; Porter, C. J.; Pouton, C. W. Using polymeric precipitation inhibitors to improve the absorption of poorly water-soluble drugs: A mechanistic basis for utility. *J. Drug Targeting* **2010**, *18* (10), 704−731.
(39) Luo, L. B.; Eisenberg, A. Thermodynamic size control of block copolymer vesicles in solution. *Langmuir* **2001**, *17* (22), 6804−6811.
(40) Mosquera-Giraldo, L. I.; Borca, C. H.; Meng, X. T.; Edgar, K. J.; Slipchenko, L. V.; Taylor, L. S. Mechanistic Design of Chemically Diverse Polymers with Applications in Oral Drug Delivery. *Biomacromolecules* **2016**, *17* (11), 3659−3671.
(41) Liu, K. J.; Parsons, J. L. Solvent Effects on Preferred Conformation of Poly(Ethylene Glycols). *Macromolecules* **1969**, *2* (5), 529−533.
(42) Mochizuki, K.; Ben-Amotz, D. Hydration-Shell Transformation of Thermosensitive Aqueous Polymers. *J. Phys. Chem. Lett.* **2017**, *8* (7), 1360−1364.

DOI: 10.1021/acs.molpharmaceut.8b00324
Mol. Pharmaceutics 2018, 15, 3236−3251